Cascading Failure Analysis With DC Power Flow Model and Transient Stability Analysis

Jun Yan, *Student Member, IEEE*, Yufei Tang, *Student Member, IEEE*, Haibo He, *Senior Member, IEEE*, and Yan Sun, *Member, IEEE*

***Abstract*—When the modern electrical infrastructure is undergoing a migration to the Smart Grid, vulnerability and security concerns have also been raised regarding the cascading failure threats in this interconnected transmission system with complex communication and control challenge. The DC power flow-based model has been a popular model to study the cascading failure problem due to its efficiency, simplicity and scalability in simulations of such failures. However, due to the complex nature of the power system and cascading failures, the underlying assumptions in DC power flow-based cascading failure simulators (CFS) may fail to hold during the development of cascading failures. This paper compares the validity of a typical DC power flow-based CFS in cascading failure analysis with a new numerical metric defined as the critical moment (CM). The adopted CFS is first implemented to simulate system behavior after initial contingencies and to evaluate the utility of DC-CFS in cascading failure analysis. Then the DC-CFS is compared against another classic, more precise power system stability methodology, i.e., the transient stability analysis (TSA). The CM is introduced with a case study to assess the utilization of these two models for cascading failure analysis. Comparative simulations on the IEEE 39-bus and 68-bus benchmark reveal important consistency and discrepancy between these two approaches. Some suggestions are provided for using these two models in the power grid cascading failure analysis.**

***Index Terms*—Cascading failure, contingency analysis, DC power flow, transient stability, vulnerability assessment.**

I. Introduction

THE modern power system is advancing towards a critical and promising intelligent generation known as the Smart Grid. This new generation is expected to integrate the efficiency, flexibility, and stability optimization benefits from the computer-based communication networks. However, it is notable that the Smart Grid cannot by pass some structural vulnerabilities in power grids. For instance, in a ripple effect known as the *cascading failure*, a single disturbance or contingency can trigger a chain effect of unpredictable and disastrous disturbances to the power grid under certain conditions [1]. Recent blackouts, e.g., the 2011 Southwest blackout in Arizona and South California [2] and the record-breaking blackout in India [3], have revealed a strong impact of critical infrastructure failures that draws the concerns of the government, the industry and the public. However, with foreseeable cost of reconstructing the whole power grid to the highest standard, the Smart Grid still has to rely on the existing electrical infrastructure despite of some of its inherent vulnerabilities [4], [5]. In addition, new vulnerability and security challenges have been posed to the grid managers as the infrastructure can become a target of cyber-physical threats [6], [7]. As a result, there is a growing call for the thorough understanding of the mechanism behind cascading failures to enhance power grid's stability.

The IEEE PES CAMS Task Force on Understanding, Prediction, Mitigation and Restoration of Cascading Failures [8] has reported a variety of simulation models that are developed for cascading failure analysis [9]–[11]. All these models focus on certain sets of assumptions to approximate the real power system, but a well-accepted model is still absent due to the complexity of interconnected power grids and cascading failures themselves. While some studies have investigated the validity of using graph theory based and complex network based cascading failure models and metrics [12]–[16], there is little literature comparing the validity of using different power system models to approximate system behavior in cascading failures. This becomes the motivation of this paper: to investigate the model comparison on two typical well-established models used to assess grid vulnerability of cascading failures, i.e., the DC power flow-based model against the transient stability analysis method.

The first type of model in comparison is the power flow model. This is based on steady-state analysis, which is widely used in studies of cascading failures to approximate AC power equations of power systems. For instance, Dobson *et al.* have proposed a stochastic ORNL-PSerc-Alaska (OPA) model [17]–[19]. Carreras *et al.* have also produced comprehensive work on self-organized criticality [20]–[22] in cascading failures using the AC power flow-based Manchester model [23], [24] and CASCADE model [25]. Compared to the AC flow models, the DC power flow-based cascading failure simulator (CFS) is powerful for its balance between model complexity and system behavior approximation [8], [26]. It utilizes the assumptions of power flow equations [27], [28] for efficient

Manuscript received October 01, 2013; revised November 05, 2013, November 06, 2013, February 04, 2014, and April 12, 2014; accepted April 29, 2014. Date of publication May 20, 2014; date of current version December 18, 2014. This work was supported in part by the National Science Foundation under grants CNS 1117314, CNS 0643532, and ECCS 1053717, and in part by the Army Research Office under grant W911NF-12-1-0378. Paper no. TPWRS-01253-2013.

The authors are with the Department of Electrical, Computer and Biomedical Engineering, University of Rhode Island, Kingston, RI 02881 USA (e-mail: jyan@ele.uri.edu; ytang@ele.uri.edu; he@ele.uri.edu; yansun@ele.uri.edu).

Color versions of one or more of the figures in this paper are available online at http://ieeexplore.ieee.org.

Digital Object Identifier 10.1109/TPWRS.2014.2322082

cascading failure simulation and assessment. Therefore, in this paper, we have implemented a well-defined CFS [29] as a typical example of steady-state cascading failure simulator.

In contrast to the power flow-based steady-state analysis, transient stability analysis (TSA) is considered to be one of the most comprehensive and complex approaches for power grid stability analysis. Based on the differential algebraic equations (DAE), they have been widely used in power system control design [30] and adopted as the validation tool for many related studies. Although TSA methods are still inadequate reproducing the events of real power outages [31], the time-domain simulations of TSA provide adequate system dynamic information. This could be incorporated into steady-state models, such as the optimal power flow (OPF) model [32], [33], for improved system security and better outage prevention.

While much literature focuses on either DC power flow-based analysis or transient stability analysis, there are few studies on the discrepancy and consistency of these two models in evaluating the impact of cascading failures. The apparent distinctions between the CFS and TSA models can not delineate that to what degree these two methodologies are consistent or different with each other in cascading failure analysis. Therefore, this paper aims to provide a reference, through illustrative comparative studies, to help determine a more appropriate model for the analysis of power grid cascading failures from case to case. To be specific, in this paper a new metric named critical moment (CM) is proposed based on the rotor angle stability and voltage stability principles of power grids. This study is expected to narrow the knowledge gap between these two well-developed models and to facilitate understanding of cascading failures in power systems.

There are two typical DC power-flow-based CFS distinguishable by their focuses. Some studies [19], [34] focus on long-term effects to first evaluate temperature and line-expansion to determine the vulnerability of a branch. Then proper control measures, e.g., vegetation management, can be applied to reduce the risk of blackouts. Meanwhile, other research places a focus on relays [29], because they are critical factors in major blackouts due to the automatic branch tripping mechanism operated by relays [35]. The relay-based CFS usually focuses on short-term effects occurring in seconds or minutes; in contrast, the long-term models run from less than an hour to a few days. For a fair comparison between the two methodologies, it is therefore more suitable for this paper to compare the relay-oriented CFS to TSA models in this cascading failure study.

In the rest of this paper, we refer to the original cascading failure simulator in [29] as the CFS, and its modified version in this paper as the DC-CFS, respectively. In addition, the DC power generation and load are denoted as P_g and P_d, respectively, where g denotes a generation bus and d a load bus; correspondingly, the complete sets of generators and load buses are denoted as G and D, respectively. The AC (reactive) power generation and load are denoted as Q_g and Q_d, respectively. Similarly, l refers to a branch and B is the set of branches, while the DC branch power flow is denoted by F. Finally, voltage magnitude and angles are denoted as V and θ, respectively.

The rest of this paper is organized as follows: Section II describes the adopted power flow-based DC-CFS for cascading failure analysis. Then Section III presents assessment of DC-CFS simulation of cascading failures that are triggered by the single-component contingency. Comparison to TSA simulation results are discussed in Section IV, where the new notion CM is defined and discussed to reveal the validity of DC-CFS. Finally, conclusions are provided in Section V.

II. DC Power Flow-Based Cascading Failure Simulator (DC-CFS)

The DC-CFS assessed in this paper is adopted from a recent study published in 2012 [29] on multi-contingency triggered cascading failure, which belongs to a family of models of cascading failure based on DC power flow assumptions without consideration of reactive power and transmission loss [22], [29], [36]–[38]. In this paper, some minor modifications are made to the original CFS for better comparison. A quick overview is provided as follows:

1) The DC-CFS implemented an additional trigger of bus contingency so that cascading failure of both bus and branch contingencies can be simulated to validate the use of DC-CFS compared to the TSA approach;
2) In the generation and load re-dispatch process of the DC-CFS, we introduced weight vectors to the generation and load buses, which can be determined empirically in advance, or adjusted adaptively according to the feedback of simulated blackout size with proper algorithms;
3) A dedicated module is designed in the DC-CFS to handle the islanding issue so that the simulation can be implemented in parallel and further islanding technique and policy can be incorporated;
4) The system failure criterion of 10% in blackout size in original CFS is canceled in the DC-CFS so that we can explore and compare the full development of a potential cascading failure process in both models. Moreover, we can also justify if this criterion is appropriate in the simulation of cascading failures;
5) Last but not least, more implementation details, including the ramping rate, the ramping period, are provided to further improve this DC-CFS dedicated for cascading failure analysis.

While these modifications are not considered as the contribution of this paper, they are adjustments to the original CFS for fair comparison between the DC-CFS and TSA model in cascading failure analysis. The whole process can be divided into four steps, each represented by a subsection (*Steps A–D*) below to describe specifications on cascading failure triggers, dispatch policy, and islanding processing. The assessment metrics are discussed in the end of this section.

A. Cascading Failure Triggers

In the DC-CFS we consider a potential cascading failure caused by both branch and bus triggers in the system. A branch trigger is the tripping of a branch, as modeled in traditional contingency analyses [13], [29], [39]. On the other hand, a bus trigger is the failure of a bus, or substation, after which no power flow is transmitted through the malfunctioned bus.

The bus trigger is less frequently studied due to rare occurrence of a complete failure of substations or power plants in

contrast to the more common cases of branch tripping. Nevertheless, a cascading failure can still be triggered by a bus failure, after which branches connecting to the failed bus is also tripped since the power will not be able to flow either *from* or *to* the failed bus [40], [41]. Theoretically, a bus contingency is more likely to result in cascading failures and cause greater damages to the grid because of the concurrent failure of multiple branches and potential direct loss of load and generation, which overruns the $N-1$ criterion. Therefore, we implement both triggers in this paper to better understand cascading failures in power systems.

B. Relay-Based Overloading Branch Tripping

Branch tripping is one of the most common factors responsible for the cascading failures [8]. Therefore, we refer to each tripping as a *cascading failure event (CFE)*, and the whole process of cascading failure is then represented by a series of CFEs. The initial contingency is numbered as CFE 0, while the following CFEs occured during a cascading failure are numbered by positive integers thereafter. When a CFE occurs, overloading may be found on a branch l whose power flow F_l exceeds its thermal rating of power flow, denoted as C_l. As critical or long-lasting overloading can cause great damage to the power transmission, the relays will respond to these overloadings by tripping dangerously overloading branches from the grid. For an overloaded branch denoted as l', the following accumulative function $O(l',t)$ from [29] determines the severeness of overloading on a branch l at time t:

$$O(l,t) = \int_{t_0}^{t} \left[F_l(\tau) - C_l\right] d\tau, \quad F_l(\tau) > C_l \tag{1}$$

where $F_l(\tau)$ is the branch power flow at time τ. Theoretically, under the steady-state assumption, $O(l,t)$ of a branch l is integrated over the duration when it is overloaded while the system remains in a steady state. As the power flow F_l will be changed by the generation and load re-dispatch after the occurrence of a CFE, t_0 and t in practice will have to be changed accordingly, which will be described later in the next subsection following (2). If the accumulation $O(l,t)$ exceeds a dangerous threshold $O_{limit}(l)$ at time $T_f(l)$, the relays will automatically trip off the corresponding branch l. This critical threshold is defined empirically based on referential scenarios as in [29]. Note that $O(l,t)$ is not the actual heat accumulated on the branch, but an accumulative function of overloading evaluated by the relays to trip dangerous branches accordingly.

C. Generation and Load Re-Dispatch

When a new failure occurs, the power transmission can be disrupted, and the balance of load and generation has to be restored via re-dispatch process [42]. Specifically, between two consecutive cascading failures in a fully-connected grid, the following re-dispatching steps are performed:

***C.1* Generation ramping**

The generation ramping consist of two scenarios:

1) If there is a generation surplus, i.e., $\sum P_g > \sum P_d$, ramp down all generators' output with a given ramping rate r.
2) If there is a generation deficit, i.e., $\sum P_g < \sum P_d$, ramp up all generators' output with the given ramping rate r until ramping is terminated;

The ramping is terminated if any of these two following conditions is met: 1) $\sum P_g \geq \sum P_d$; or 2) the output of a given generator has reached its capacity $P_{max}(g)$;

***C.2* Generator tripping/Load shedding**

Similar to the generation dispatch, there are also two corresponding processes to handle the surplus and deficit, respectively:

1) If the surplus still exists after ramping, then the generators with minimal non-zero importance will be instantly tripped one by one in the grid until $\sum P_g \leq \sum P_d$;
2) If the desired balance ($\sum P_g = \sum P_d$) is still not met after a certain amount of time T_{ramp}, the load on the bus with the minimal non-zero importance will be shed one by one, until the load-generation balance is established;

***C.3* Power flow update**

After the ramping and shedding process, the power flow on each branch is instantly recalculated and redistributed to set up a new system operating point.

In this procedure, the ramping in *Step C.1* tries to resolve any imbalance between generation and load caused by cascading failure. In both scenarios, we assumed all generators ramp up or down with a uniformed maximal ramping rate r with respect to their capacity. As this ramping process can be interrupted by a new CFE in the system, the duration of generation ramping period between two CFEs, denoted as T_{ramp}, is determined by the following equation:

$$T_{ramp} = \min_{l \in L} \{T_f(l)\} \tag{2}$$

where $T_f(l)$ corresponds to the dangerous threshold $O_{limit}(l)$ as aforementioned. No failure occurs during this period T_{ramp}, and the power grid is assumed to stay in a steady-state. Therefore, the accumulative overload $O(l,t)$ in (1) is integrated from t_0, the moment when a new CFE is observed, to $t_0 + T_{ramp}$, the moment when the next CFE occurs in the system. In this way, if a new CFE occurs in the system, the actual value of t_0 is automatically reset to the time when this CFE occurs, and t is set to $t_0 + T_{ramp}$ when T_{ramp} is calculated by (2). This allows the DC-CFS to directly use T_{ramp} as a step time in simulation instead of using small, unit step intervals in classic transient stability models, which can be computationally expensive otherwise.

During the ramping period, a system can resume stable if the generation deficit or surplus is eliminated; however, if the desired balance is not met through ramping, then a generator tripping and/or load shedding is performed in *Step C.2* as the last resort to ensure the stability of system. The importance of a generation bus Y_g is determined by the product of its generation P_g and a weight vector W_g, i.e., $Y_g = W_g \cdot P_g$; similarly, the importance of a load bus is calculated by $Y_d = W_d \cdot P_d$.

Afterwards, the system operation point is updated in *Step C.3* to continue the iterative simulation process. This procedure follows the general principle to maximize the adjustment on the generation side while minimize the impact on the load/consumer's side as long as the power system remains stable.

D. Handling Islanded Sub-Grids During Cascading Failures

During the process of a cascading failure, an originally fully connected grid can be disintegrated into several islands, which can still maintain independent operation. Each island has independent topology, operating point, and potential cascading failures that continue to propagate therein. Instead of assigning a new CFS for each new island, in this paper we used a more direct tactic to efficiently simulate cascading failure in islands of a power grid without increasing the implementation difficulty.

Specifically, an island emerged when a CFE breaks down the grid is rendered as a new fully-connected sub-grid that carries the most recent system operating point in corresponding segment. If generation and load are not balanced in an island, the simulator re-dispatches the load and generation and recalculates power flow through *Step C.1* to *Step C.3* to establish a new balanced operating point, and obtains corresponding value of T_{ramp} in each island if a new CFE occurs.

As islands may be further broken down when cascading failure continues to propagate, it is necessary to synchronize among different cascading failure processes in different sub-grids during simulation. Therefore, when the values of T_{ramp} for all current sub-grids are obtained, we will use the minimum of them as a global time step ΔT to advance the simulation:

$$\Delta T = \min_i \{T_{ramp}(i)\} \tag{3}$$

where $i = 1, 2, \ldots, K$, and K is the number of existing sub-grids. It is notable that two consecutive values of ΔT may be obtained from different islands during the simulation, so the sequence and location of the events is also recorded accordingly. Also, because ΔT is the minimum of T_{ramp} across different islands, by definition every island still remains in steady state with their own operating points.

This sub-grid handling is beneficial because the number of islands emerging during a cascading failure is unknown in advance. This uncertainty causes a high computation overhead for the simulator to process a time-variant number of islands simultaneously. From *Step A* to *Step D*, cascading failures in all existing islands will be simulated recursively until no overloading is further observed. As a summary, Fig. 1 shows the general process of the DC-CFS simulation.

E. Assessment Metric for DC-CFS

To assess the impact of cascading failures with DC-CFS, we choose the *blackout size* as the assessment metric of a cascading failure. Denoted as ΔP, it is defined as the *percentage* of overall loss of load (measured in real power) with respect to the original loading

$$\Delta P = \frac{\left[\sum_{d \in D_0} P_{D_0} - \sum_{d \in D'} P'_{D'}\right]}{\sum_{d \in D_0} P_{D_0}} \tag{4}$$

where D_0 and D' are the sets of load buses in the original grid and the final grid, respectively. P_{D_0} and $P'_{D'}$ are the corresponding load remaining in each grid, respectively. It is also notable that the final load loss, as a result of generation and load re-dispatch in *Step C*, is equivalent to the loss of generation as the system is designed to be balanced after *Step C*.

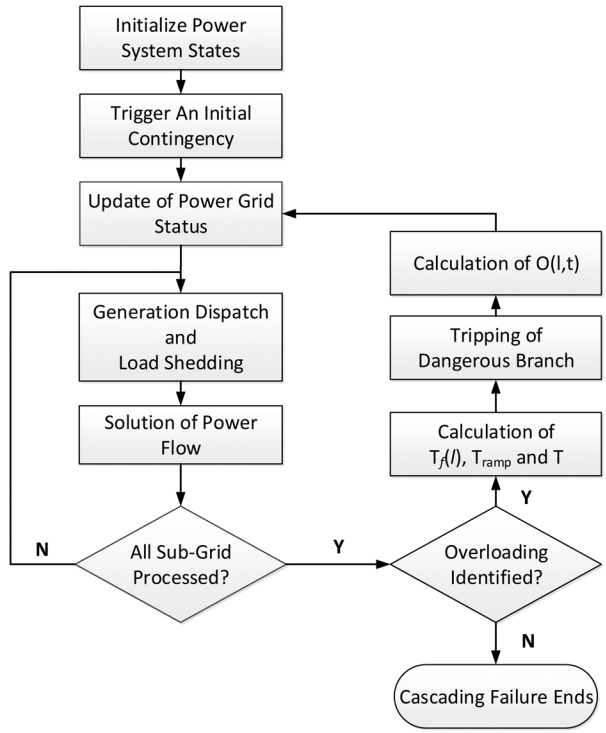

Fig. 1. Flowchart of DC-CFS.

According to the model described above, we decompose the final blackout size ΔP into three parts. First, if a contingency is initially triggered on a load bus that has a non-zero load, the load on that bus will instantly lost, which is referred to as the direct loss of real power. Secondly, immediately after the initial contingency, the blackout size is contributed by the system's first re-dispatch and shedding process in *Step C* as an emergent response. Since there is limited time to react to the abrupt contingency, some load will be shed in this emergent response. Third and last, after the re-balance of load and generation, a potential cascading failure triggered by overloading branches will further increase the loss of load.

In addition to the blackout size ΔP, the number of load buses affected during the cascading failure (ΔN_L) is also assessed as comparative metrics of the cascading failure impact. It is measured as the number of load buses whose load is either completely or partially shed during the cascading. The correlation efficient of ΔN_L and ΔP will be evaluated for comparison in following simulations.

III. Assessment of Cascading Failures With DC-CFS

A. Simulation Setup

In this paper, the DC-CFS is implemented in MATLAB and the MATPOWER [27] toolbox is used to calculate DC power flow in the benchmark. The standard IEEE 39-bus system is also chosen from MATPOWER as a benchmark system to evaluate the DC-CFS. This system has a total load of 62.54 p.u., and it contains 39 buses (10 of which are generation buses) and 46 branches whose capacity C_l is also given in the benchmark.

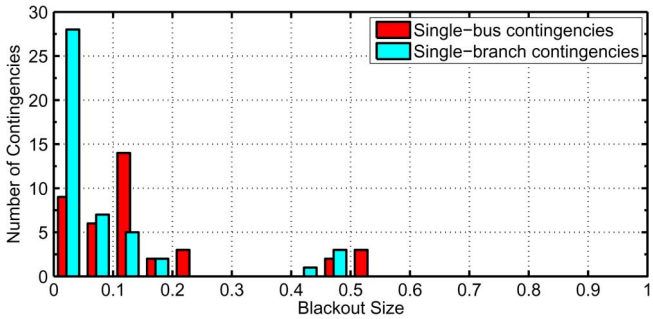

Fig. 2. Histogram of blackout size in single-bus and single-branch contingencies.

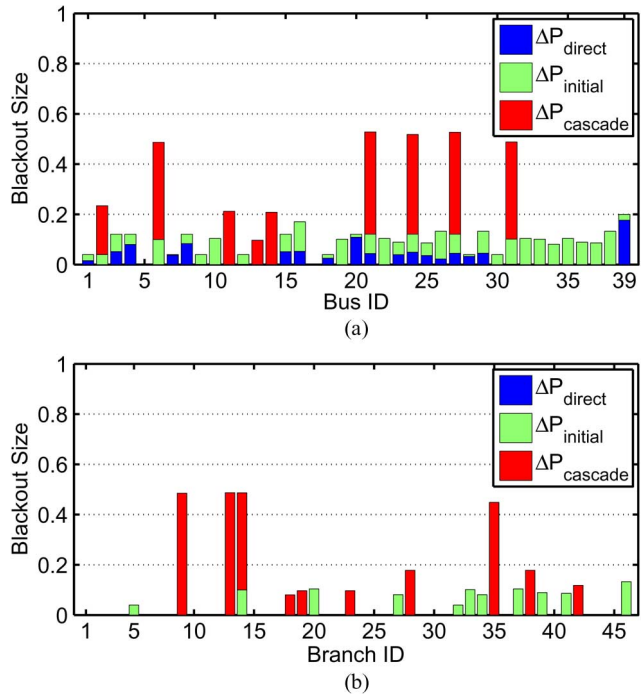

Fig. 3. Decomposition of single-bus and single-branch triggered blackout sizes. The three bars, stacked from the bottom to the top, correspond to the direct load loss, the loss after the initial re-dispatch, and the loss caused by the cascading failure, respectively. Note that there is in fact no ΔP_{direct} for single-branch triggers.

It represents the New England area power system, of which a single bus (Bus 39) represents the regional system's interconnection to the rest of US/Canada. As one of the most widely used benchmarks in power system studies, it is a suitable general representation of typical regional power transmission networks.

In addition, to reflect the modern power system standard, we referred to a recent performance standards of generators [43] to assign the ramping rate. As the real power generation of all generators in the 39-bus system are in fact greater than 250 MW (2.5 p.u), we simply choose r as 5%/min with respect to each generator's capacity. Since we do not have a practical reference of the importance of buses, all generation buses are assigned equal importance ($W_g = 1/N_G$); the same for all load buses ($W_d = 1/N_D$). As a result, Y_g and Y_d are proportional to the generation and load of corresponding types of buses, respectively, and so the simulator trips the generator with minimum non-zero generation and then sheds the non-zero load in the grid when necessary. These values of r, W_g, and W_d can be adjusted accordingly when detailed information is obtained in real power system applications. If such information is not available, these weights can also be adjusted heuristically according to the blackout size simulated in the DC-CFS as well as other stability constraints in consideration. This way it also better approximates a real power system and help the goal of minimizing the impact of cascading failure. Finally, as mentioned before, we refer to [29] to calculate the critical threshold $O_{limit}(l)$ with $T_{ref} = 5$ s and $F_l = 150\% \times C_l$. With all these settings, the DC power flow-based simulation results are presented as follows.

B. Assessing Impact of Cascading Failures With the 39-Bus System

First, we illustrate the histograms of the final blackout size of both single bus and single branch contingency in Fig. 2. As discussed in Section II-A, given the same number of simultaneous contingencies, single-bus contingencies should in general yield greater cascading failure damage than branch contingencies. The distributions in Fig. 2 are consistent with this assumption. Roughly 61% of the 39 single-bus contingencies and 24% of the 46 single-branch contingencies lead to a blackout size greater than 10% of the overall load in the system. It is also notable that while the majority of the blackout sizes are no greater than 25%, some critical contingencies still result in the loss greater than 40%.

In addition to assessing the overall blackout size of real power caused by single-component contingencies, Fig. 3 illustrates the decomposition of overall blackout size in single-bus and single-branch contingencies, respectively, where different components of a blackout size are shown as stacked bars representing different components in final blackout sizes. The first type of bars ΔP_{direct} on the bottom is the direct load loss on the victim buses; the second type of bars $\Delta P_{initial}$ in the middle represents the load loss after the initial emergent re-dispatch right after the contingency; finally, the last type of bars $\Delta P_{cascade}$ on top corresponds to the fraction of blackout sizes contributed by the triggered cascading failures.

As shown in Fig. 3(a), in single-bus contingencies the initial re-dispatch adds a significant amount to the blackout size to the direct loss of load buses, which is observed on most generation buses (Bus 30 to 38) and some load buses (Bus 6, 10, 16, etc.). The generation-load combined Bus 39 is the only exception as it carries the largest generation and load simultaneously in the system. As an equivalent bus of interconnection to the rest of US/Canada, Bus 39 in this benchmark provides 15.88% of the generation and consumes 17.65% of the power in this system, resulting in a significant direct impact to the system when it fails even without a cascading failure. Nonetheless, from Fig. 3(a) it is still shown that the cascading failure triggered by less loaded buses is responsible for the most severe single-bus contingencies blackouts. Meanwhile, the type of bus is not closely related to the eventual blackout size, as the most severe single-bus contingencies ($\Delta P > 20\%$) can be found on both load-only buses (Bus 6, 21, 24, 27) and load-generator bus (Bus 31). In fact,

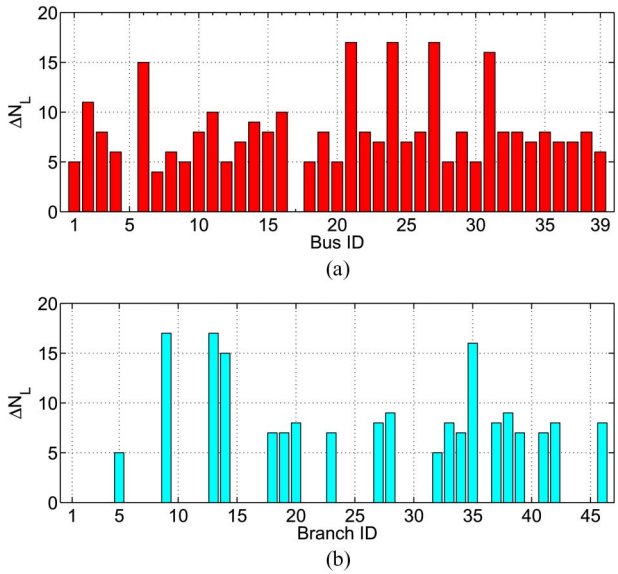

Fig. 4. Number of affected load buses according to (a) single-bus triggers and (b) single-branch triggers of DC-CFS, respectively.

because the type of a bus can be defined interchangeably by altering the net injection of the given bus without changing the overall system dynamics, it does not have a definite influence on the eventual blackout size. Instead, the decomposition of ΔP in Fig. 3(a) has shown that cascading failure plays a more important role in the final impact.

Similar observation can be found in Fig. 3(b) for single-branch contingencies. Although for branch contingencies, there is no direct loss of power ΔP_{direct} on branches, the re-dispatch still contributes to some blackout sizes that reach the similar scale as the bus-contingency blackouts without a cascading failure. However, in the most severe cases, the cascading failure is still the major factor in severe blackouts, which raises some ΔP to nearly 50%. For both types of triggers, we have observed that cascading failures contribute significantly in the major blackouts caused by a single-component contingency.

In addition to the blackout size ΔP, we have also evaluated the number of load buses affected in the cascading failures using DC-CFS. The number of load buses affected by a cascading failure (ΔN_L) is shown in Fig. 4 with both types of triggers. The correlation coefficients of ΔP and ΔN_L are $\rho_{pl,bus} = +0.9365$ for buses and $\rho_{pl,branch} = +0.9278$ for branches, respectively. The results indicate a relatively high correlation between the blackout size and the number of buses that subject to load shedding during the cascading failures, which is reasonable as the bus with the minimal load will be directly tripped when generator ramping cannot achieve the load-generation balance.

As a summary of this section, from the simulation results and analysis above, the DC-CFS proves to be a useful tool to understand the vulnerability of a power system against cascading failures. Information of the final impact, cascading failure development as well as contributing factors can be obtained more efficiently with the DC-CFS, which is especially helpful if it is extended to a bulk power system or a detailed regional grid that has much greater number of substations and transmission lines in the system.

IV. Comparative Study Between DC-CFS and TSA-Based Cascading Failure Analysis

While the DC-CFS simulation shown above presented interesting and important information on potential blackout sizes of cascading failures, it is certainly critical to understand how precise these vulnerability assessments are in comparison to some more complex methodologies. As mentioned before, the DC power flow model is a proper representation of high-voltage low-load power grids [26] with a good balance between the computational efficiency and model complexity. It certainly provides important information of power system behavior in cascading failures. However, it does not consider the reactive power and voltage characteristics in a complex power system, and a steady-state assumption can fail to hold in the complex dynamics of a real power system. Therefore, we presented a comparative study between the DC-CFS and transient stability analysis (TSA) to understand the discrepancy and consistency between them for cascading failure analysis. The TSA model is implemented in the Power System Analysis Toolbox (PSAT) software, a popular open source toolbox for the research on both static and dynamic analysis of power systems [44].

In addition to the IEEE 39-bus system shown in Fig. 5, we also implemented the IEEE 68-bus system in PSAT as an additional benchmark for more comprehensive comparison, as shown in Fig. 7. The additional system is a representation of the New England and the New York power system, with three buses as the equivalent of three external regions connected to these two regional power grids. As an extension to the 39-bus system, the 68-bus system has a significantly larger total load of 176.21 p.u., and both variances of power generation and load consumption also become greater than the 39-bus system. This more complex network can pose greater challenge to the DC-CFS as discussed below. All parameters used in PSAT can be found in publications for the 39-bus system [45], [46] and the 68-bus system [47], respectively. There is no direct generation dispatch or load shedding in PSAT, and branch tripping is simulated upon each occurrence of CFE identified by the DC-CFS. Numerical comparison between two models are presented below to reveal their consistency and discrepancy in the simulation of cascading failures.

A. Model Comparison Through A Case Study

To illustrate the consistency as well as discrepancy between the DC-CFS and the TSA model, a comparative case study of a single-branch contingency in the 39-bus system is first presented as follows. We choose the cascading failure caused by the tripping of Branch 14 (from Bus 6 to Bus 31) as a baseline for the comparative study. This branch failure isolates Generation Bus 31 from the grid, which has been shown previously as a severe cascading failure in the system. According to the DC-CFS simulation result, after the cascading failure has been triggered, subsequent branch tripping has been found on Branch 13, 9, 6, 1, and 23 before the failure terminates. We record this sequence of CFEs with the moments of occurrences in DC-CFS, and then set up the simulation of identical branch tripping at the same moments in PSAT. The location and occurrence time of these CFEs are shown in Fig. 5. Then we observe whether there

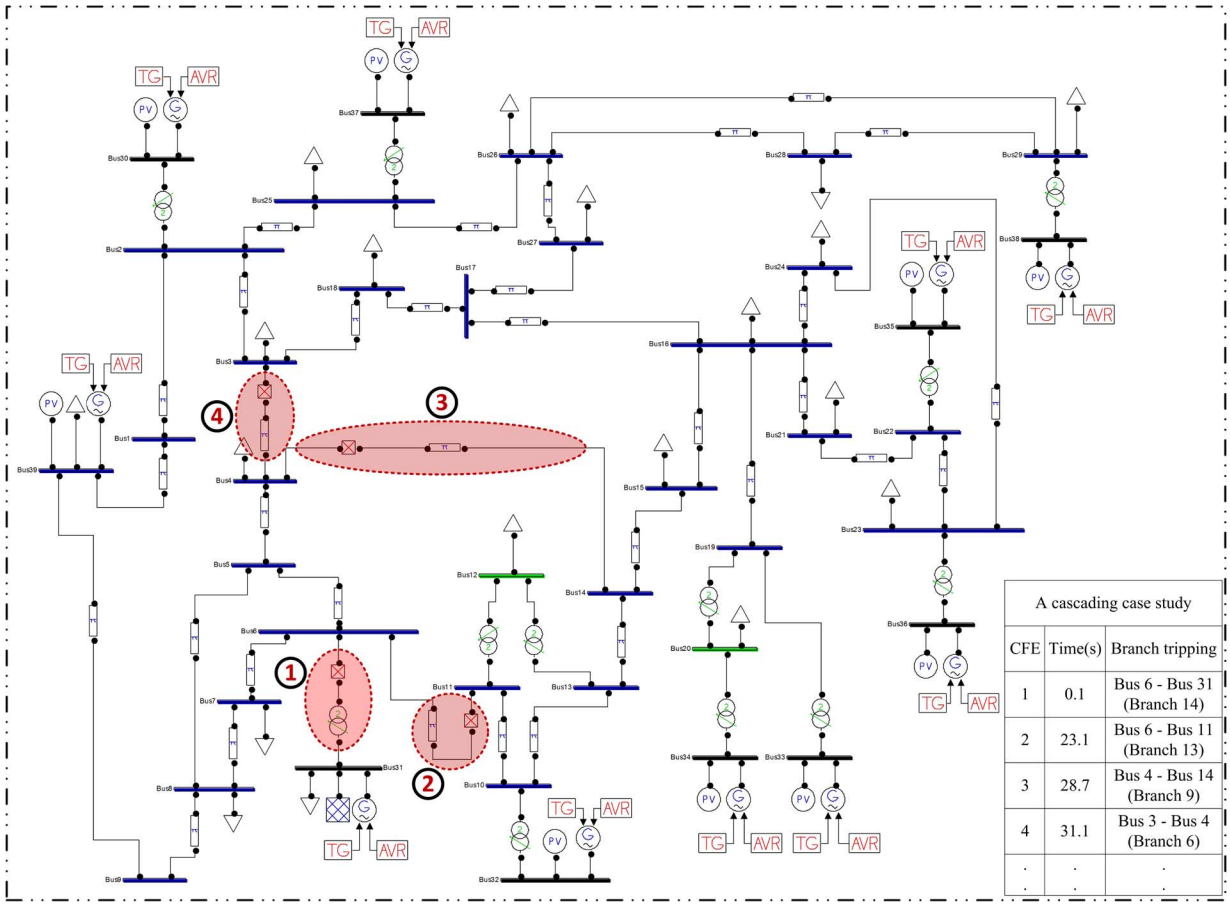

A cascading case study		
CFE	Time(s)	Branch tripping
1	0.1	Bus 6 - Bus 31 (Branch 14)
2	23.1	Bus 6 - Bus 11 (Branch 13)
3	28.7	Bus 4 - Bus 14 (Branch 9)
4	31.1	Bus 3 - Bus 4 (Branch 6)
.	.	.
.	.	.

Fig. 5. Typical cascading failure on IEEE 39-bus system. Branches affected in the cascading failure are highlighted.

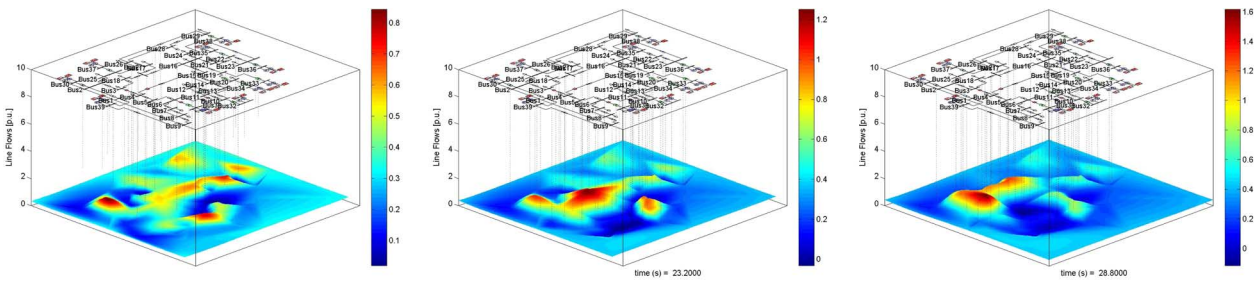

(a) (b) (c)

Fig. 6. Transmission line load rate distribution in cascading failure propagation at different moments. (a) System transmission line flows before cascading. (b) At CFE 2, Branch 13 from Bus 6 to Bus 11 is tripped. (c) At CFE 3, Branch 9 from Bus 4 to Bus 14 is tripped.

is a consistent trend of power re-distribution and branch overloading, and if so, to what extent this consistency holds during the cascading failure.

The corresponding line load rate distribution after each CFE is partially visualized in Fig. 6, and the initial system branch flow is shown in Fig. 6(a). After the initial failure of Branch 14 (CFE 1), the active power transmission on Branch 13 increased immediately. This is because Branch 14 is linked to Load Bus 1 with a generator Bus 31, whose failure requires the generator to provide more power to Load Bus 7, Load Bus 8, and Load Bus 4 through Branch 13 simultaneously, resulting in a severe overloading condition that forces the relay to trip off Branch 13 in CFE 2 after 23.1 s. Fig. 6(b) shows the system line load rate change after the tripping of Branch 13, in which the active power transmission on Branch 9 increased suddenly. The reason is that Branch 13 and Branch 9 are two branches connected the left generation area to the right load area. The tripping of Branch 13 will increase the Branch 9's transmission burden. As a result, Branch 9 was consequently tripped by a relay in CFE 3 at 28.7 s after the initial tripping. Until this point, simulation results remain consistent between the two models despite that they are based on different power flow assumptions and the regulation, i.e., TG and AVR, is only performed in the PSAT simulation.

Upon the next occurrence of CFE, however, the system dynamics begin to change. Although in Fig. 6(c), the most severe overloading is still observed on Branch 6 for both DC-CFS and TSA models, in Fig. 8(a) and (b), the system voltage has already started to collapse after CFE 3, making following simulations in two models diverge into different flow distributions. As some

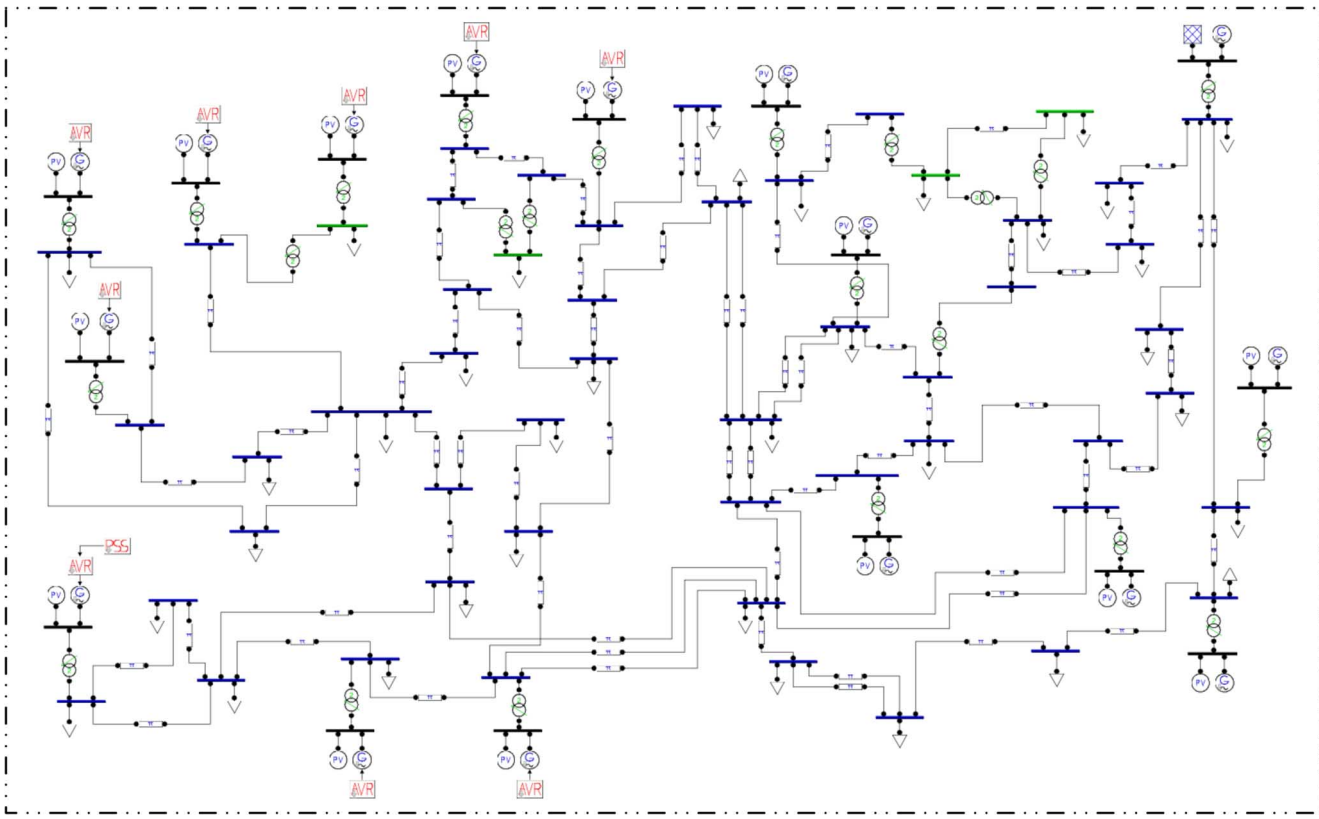

Fig. 7. Diagram of IEEE 68-bus system implemented in PSAT.

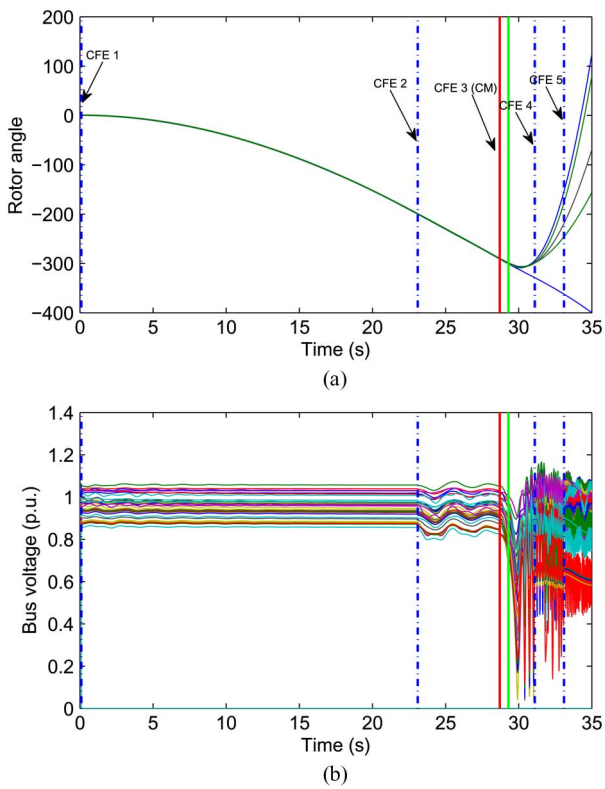

Fig. 8. (a) Rotor angles and (b) bus voltages in the study case. Each curve in (a) represents a generator and in (b) a bus in the 39-bus system. Bus 31 (which is also Generator 2) is excluded as it is immediately isolated after Branch 14 is tripped. The vertical dotted lines represent CFEs and the vertical solid line represents the CM.

bus voltages dropped to a relative low value and some generators start to desynchronize after CFE 3, the system became unstable as the bus voltages began to oscillation till the end of simulation. If this situation happens in real power system, grid operator will trip some generators to prevent further damage to the machines caused by desychronization. As a result, the branch line load rate distribution in simulation also began to diverge between these two models from the next CFE. Specifically, the active power transmission on Branch 16 increased dramatically in the TSA model, while the DC-CFS simulation suggested that the next branch to be tripped should be Branch 1. As a summary, for this cascading failure triggered on Branch 14, the steady-state assumption no longer holds after CFE 3 due to the significant change in the power grid dynamics. The importance of CFE 3 in this example leads to the concept of CM as an index of consistency, which is described below.

B. Critical Moments in Model Comparison

With the case study above, we can now define the CM in a more generic way for comparison between the two models. To define the CM numerically, we refer to two principles of power systems, i.e., the rotor angle stability and voltage stability as the criteria.

Considering the following two numeric criteria in simulation:

1) The maximal difference between any two rotor angles is greater than 10°;
2) The voltage of any bus deviates from its original voltage in p.u. by 10%.

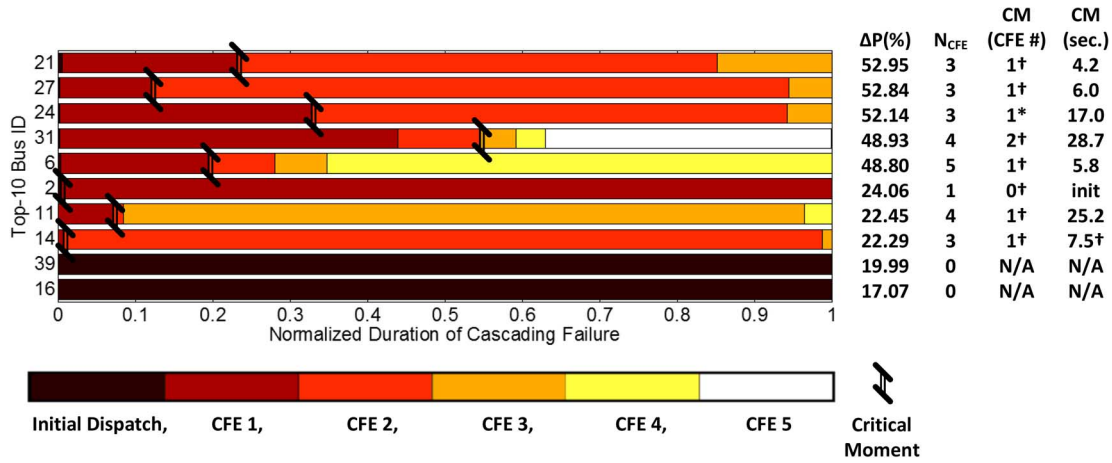

(a)

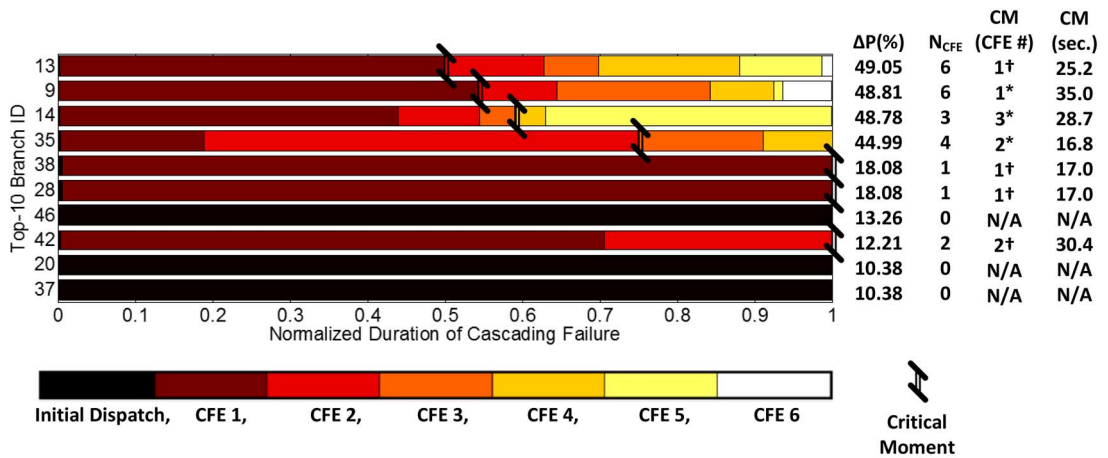

(b)

Fig. 9. Normalized T-Diff figure of the top-10 (a) buses and (b) branches with the greatest blackout size in the 39-bus system. "init." denotes right after the initial dispatch, and "N/A" denotes that the moment does not exist. The superscripts next to CM indicate whether the criterion of rotor angle stability (marked with †) or the criterion of voltage stability (marked with $*$) is met when the corresponding CM is obtained.

Then the CM is defined as the most recent CFE that occurs before the point when either 1) or 2) is met. As a example, if criterion 1) or 2) is satisfied at a moment τ between CFE k and CFE $k+1$ in a cascading failure simulated by the DC-CFS, then CFE k is selected as the CM after which the steady-state assumption does not hold for the DC-CFS.

It is notable that for most of the research on transient stability, stability criteria can vary among different benchmarks and different methods, e.g., change of sign of PEBS or an arbitrary value, such as π [32]. In this study, both thresholds are chosen empirically based on the following considerations. For criterion 1), according to [48], the angular difference depends on the power-angle relationship, where it demonstrates a highly nonlinear characteristic. For large-disturbance rotor angle stability (corresponding to small-disturbance or small-signal rotor angle stability), the time frame of interest in transient stability studies is usually 3 to 5 s following the disturbance, i.e., the most recent CFE before the divergence. In such a short time frame, it will be reasonable to set "10 degrees" as the criterion to determine the critical moment. For criterion 2), we refer to [30], which states that when the voltage drop below 85% to 90% of its nominal value, more motors may drop out consequently and lead to a cascading effect if the original cause of voltage drop remains unsolved. Therefore, we choose the moment when the voltage drops to 90% of nominal value, i.e., the 10% deviation, to determine CM with criterion 2).

Although the actual moment τ when one of the criteria is met can also be rendered as a critical point in simulation, by defining CM as a CFE that corresponds to a failure event in the system instead of a continuous time value, it is more intuitive and convenient to keep track of the CFEs. With the above definition, we have calculated the CMs for the top ten single-component contingencies of both types on IEEE 39-bus and 68-bus system, respectively.

First, for the 39-bus system, the consistency and discrepancy are visualized with a new figure called a time-domain difference (T-Diff) plot shown in Fig. 9. In this visualization, we selected the top-10 most severe blackouts of single-branch contingencies according to the DC-CFS model and illustrated their normalized duration and CMs in the bar graph. The occurrence time of each CFE in each cascading failure is normalized by their overall duration, respectively. In this way, the horizontal bars represent the series of CFEs for the top-10 cases in the time-domain. The corresponding blackout size ΔP, the total number of CFES (N_{CFE}), the CMs and their actual time of occurrence are listed to the right of the bar graph with the legends shown under

TABLE I
CRITICAL MOMENT AND VIOLATION MOMENT OF TOP-10 CONTINGENCIES IN THE 68-BUS SYSTEM

Rank	**Bus**	ΔP (%)	N_{CFE}	CM (CFE #)	CM (seconds)	**Branch**	ΔP (%)	N_{CFE}	CM (CFE #)	CM (seconds)
1	17	81.84	12	6*	4.1	74	79.84	13	1†	1.7
2	13	79.84	13	1†	1.7	70	70.79	14	1†	1076.5
3	12	70.79	14	1†	1076.5	78	62.37	8	1†	1.6
4	16	62.37	8	1*	1.6	45	51.27	13	2†	2.9
5	36	61.19	12	1*	0.8	71	40.66	9	2†	10.8
6	61	49.58	14	4†	8.3	56	33.82	4	2†	4.6
7	15	40.66	9	2†	10.8	57	33.79	4	2†	6.2
8	51	38.11	4	2*	4.0	72	30.85	7	1†	1.3
9	50	35.28	4	2*	4.0	83	25.12	9	1†	5.1
10	14	30.85	5	1*	1.3	8	19.58	3	2†	9.7

it. The superscripts next to CM indicate whether the criterion of rotor angle stability (marked with †) or the criterion of voltage stability (marked with $*$) is met when the corresponding CM is obtained.

As shown in Fig. 9, the CMs of bus-contingencies on average are relatively smaller than those of the single-branch cases. In other words, the duration in which the two models are consistent with each other is relatively longer in single-branch cases. This is reasonable as the tripping of buses usually do not follow the $N-1$ security standard in cascading failures, and so they may lead to more significant damage to the system stability and results in earlier CM than the branches.

Meanwhile, for some branch contingencies (Branch 28 and 38), consistency between the two models remains through out the whole cascading failure process. In these less complex cases, the DC-CFS can be utilized for its computational efficiency in cascading failure analysis. For the contingencies that did not result in a cascading failure (indicated by *Init.*), there is no CM between the two models, because the system always stays in a steady state after the initial contingency.

Results of CMs for the 68-bus system can be found in Table I with the same notation as in Fig. 9. The top-10 severe contingencies all lead to subsequent cascading failures according to the DC-CFS, and corresponding blackout sizes ΔP are comparably larger than that of the 39-bus system. It is also notable that some single-branch contingencies yield identical CMs as the single-bus contingencies in the 68-bus system, as each of these branches is the only branch connecting the corresponding bus to the rest of the power grid.

From Table I, it is also observed that the CMs in single-bus contingencies are relatively short compared to single-branch contingencies, which is consistent with the 39-bus system. However, although the total number of CFEs becomes greater in the 68-bus system, the CMs of the top-10 single-branch contingencies turn out to be relatively smaller compared to the 39-bus system. The major reason is that some generators (e.g., Bus 12, 13, 14, 15, and 16) are providing at least 10 p.u. of power to the rest of the grid, and the load of buses are also significantly greater (e.g., 4 buses have load greater than 10 p.u., and the maximal load is as large as 60 p.u.). This causes extremely imbalanced burden on a number of buses in the 68-bus system, while the rest of the grid operates in a state with more redundancy. The contingencies triggered on these components result in more severe damage to the system, and so the stability is lost more easily compared to the 39-bus system where no generator therein has an output greater than 10 p.u. and the maximal load is only 11 p.u. In other words, as the CM is defined by two stability criteria, it is thereby more likely to observe a smaller CM of a given contingency if the contingency leads to a greater impact to the system's stability.

As a summary, when the oscillation or disturbance is confined within a certain range, the power flow-based simulator can well approximate the power system behavior. However, when cascading failures continue to develop, the power flow-based CFS can fail in capturing the actual power system behavior as the steady-state assumption does not hold any more. In this case, TSA models are more suitable for the simulation of power system behavior so that proper critical control action can be taken to address severe power grid disturbances. For very large scale benchmarks with thousands of buses, criteria that render a power grid has reached a system failure can also be considered alternative strategy to evaluate the impact or risk of cascading failures. For instance, in the original CFS [29], the simulation of a cascading failure is terminated when the blackout size reaches 10%, which can help limit the discrepancy caused by the loss of dynamic stability in the system. The CM proposed in this paper can be further developed and utilized to determine such threshold of blackout size accordingly to take the advantage of the simulation efficiency of DC-CFS for bulk power systems. Meanwhile, as there is still a certain degree of consistency between the DC-CFS and TSA models despite the differences therein, the DC-CFS model can still be utilized for applications such as early stage intervention and mitigation of cascading failures, if the system has been designed with sufficient stability margin, e.g., greater transmission capacity or fault tolerance, against these severe single-component contingencies.

V. CONCLUSIONS

In this paper, we implemented a modified DC power flow-based cascading failure simulator to evaluate its utilization in the contingencies triggered by both bus and branch failures. Simulations on the IEEE 39-bus system were presented to illustrate the utilization of DC-CFS from multiple perspectives. Then simulation results of DC-CFS were compared and validated against the TSA approach with two benchmarks (IEEE 39-bus and 68-bus system) implemented in power system analysis toolbox (PSAT). A new concept, i.e., the

CM, is proposed and illustrated to measure important consistencies and discrepancies between these two well-established methodologies, which aims to facilitate a more comprehensive understanding of cascading failures in power systems.

Although built with only DC power flow assumptions, the DC-CFS is able to assess vulnerability of power grids in the early stage of cascading failures, as discussed in the paper. Informative details of cascading failure development can be revealed from different perspectives including the size, the contributing factors and the duration of cascading failures. However, as the DC-CFS is utilizing the steady-state assumption to replace the complex transient dynamics of power systems, if the cascading failure violates the power system dynamic stability principle, then the underlying steady-state assumption behind DC-CFS will not hold and the simulator will fail to capture the power system therein.

The CM presented in this paper illustrates the strength and limitation of DC power flow-based steady-state model in cascading failure analysis. As a model with a number of simplifications of complex power system dynamics, the DC-CFS certainly is able to acquire important information regarding the development and final impact of cascading failures. However, as discrepancy between these two models emerges in cascading failure simulation when the impact to the system dynamic stability becomes significantly large, the DC power flow-based models shall be carefully used to assess the impact of cascading failures after severe system contingencies. It is notable that this definition of CM can be further utilized for comparisons between other power system models, including the long term stochastic models when proper timing information is provided.

It is also notable that the calculation of CM in this paper still requires simulation of TSA model that will increase the computation overhead. While the major contribution of this paper is to evaluate the discrepancy and consistence between two models rather than to compete with pure DC-CFS on computation efficiency, it is desirable that CM can be determined independently for real world applications. This will be the primary focus of our future work. Also, some of the parameters, e.g., the choice of T_{ref} and F_l in the calculation of $O_{limit}(l)$, the ramping rate r in the re-dispatch procedure, and the branch capacity C_l of the benchmark system all have potential influence on the value of CM [13], [40]. This reflects the complex nature of power system and cascading failure itself, which will consist of our focus in the next stage to evaluate the significance of their influence on CM. Furthermore, we will also consider an extension to the AC power flow-based cascading failure simulator (AC-CFS) and compare this complex-power based model to the TSA approach. Then a hybrid model of the AC-CFS and the TSA model combining the strength of both models with proper visualization [49] can be beneficial to power grid operators, on which more comprehensive control policies and preventative techniques like early warning signals [50] can be further developed.

REFERENCES

[1] A. Wang, Y. Luo, G. Tu, and P. Liu, "Vulnerability assessment scheme for power system transmission networks based on the fault chain theory," *IEEE Trans. Power Syst.*, vol. 26, no. 1, pp. 442–450, Feb. 2011.

[2] Arizona-Southern California Outages on September 8, 2011: Causes and Recommendations, Apr. 2012, Tech. Rep.

[3] Report of the Enquiry Committee on Grid Disturbance in Northern Region on 30th July 2012 and in Northern, Eastern & North-Eastern Region on 31st July 2012, Aug. 2012, Tech. Rep.

[4] X. Yu and C. Singh, "A practical approach for integrated power system vulnerability analysis with protection failures," *IEEE Trans. Power Syst.*, vol. 19, no. 4, pp. 1811–1820, Nov. 2004.

[5] Y. Zhu, J. Yan, Y. Sun, and H. He, "Revealing cascading failure vulnerability in power grids using risk-graph," *IEEE Trans. Parallel Distrib. Syst.*, to be published.

[6] Y. Mo, T.-J. Kim, K. Brancik, D. Dickinson, H. Lee, A. Perrig, and B. Sinopoli, "Cyber-physical security of a smart grid infrastructure," *Proc. IEEE*, vol. 100, no. 1, pp. 195–209, Jan. 2012.

[7] S. Sridhar, A. Hahn, and M. Govindarasu, "Cyber-physical system security for the electric power grid," *Proc. IEEE*, vol. 100, no. 1, pp. 210–224, Jan. 2012.

[8] M. Vaiman, K. Bell, Y. Chen, B. Chowdhury, I. Dobson, P. Hines, M. Papic, S. Miller, and P. Zhang, "Risk assessment of cascading outages: Methodologies and challenges," *IEEE Trans. Power Syst.*, vol. 27, no. 2, pp. 631–641, May 2012.

[9] R. Baldick, B. Chowdhury, I. Dobson, Z. Dong, B. Gou, D. Hawkins, H. Huang, M. Joung, D. Kirschen, F. Li, J. Li, Z. Li, C.-C. Liu, L. Mili, S. Miller, R. Podmore, K. Schneider, K. Sun, D. Wang, Z. Wu, P. Zhang, W. Zhang, and X. Zhang, "Initial review of methods for cascading failure analysis in electric power transmission systems IEEE PES CAMS task force on understanding, prediction, mitigation and restoration of cascading failures," in *Proc. 2008 IEEE Power and Energy Society General Meeting—Conversion and Delivery of Electrical Energy in the 21st Century*, 2008, pp. 1–8.

[10] M. Vaiman, K. Bell, Y. Chen, B. Chowdhury, I. Dobson, P. Hines, M. Papic, S. Miller, and P. Zhang, "Risk assessment of cascading outages: Part 1—Overview of methodologies," in *Proc. 2011 IEEE Power and Energy Society General Meeting*, Jul. 2011, pp. 1–10.

[11] M. Papic, K. Bell, Y. Chen, I. Dobson, L. Fonte, E. Haq, P. Hines, D. Kirschen, X. Luo, S. Miller, N. Samaan, M. Vaiman, M. Varghese, and P. Zhang, "Survey of tools for risk assessment of cascading outages," in *Proc. 2011 IEEE Power and Energy Society General Meeting*, Jul. 2011, pp. 1–9.

[12] J. Yan, Y. Zhu, H. He, and Y. Sun, "Multi-contingency cascading analysis of smart grid based on self-organizing map," *IEEE Trans. Inf. Forensics Security*, vol. 8, no. 4, pp. 646–656, 2013.

[13] J. Yan, H. He, and Y. Sun, "Integrated security analysis on cascading failure in complex networks," *IEEE Trans. Inf. Forensics Security*, vol. 9, no. 3, pp. 451–463, Mar. 2014.

[14] P. Hines, E. Cotilla-Sanchez, and S. Blumsack, "Topological models and critical slowing down: Two approaches to power system blackout risk analysis," in *Proc. 2011 44th Hawaii Int. Conf. System Sciences (HICSS)*, 2011, pp. 1–10.

[15] P. Hines, E. Cotilla-Sanchez, and S. Blumsack, "Do topological models provide good information about electricity infrastructure vulnerability?," *Chaos: Interdiscipl. J. Nonlin. Sci.*, vol. 20, no. 3, pp. 033 122–033 122, 2010.

[16] M. Ouyang, "Comparisons of purely topological model, betweenness based model and direct current power flow model to analyze power grid vulnerability," *Chaos: Interdiscipl. J. Nonlin. Sci.*, vol. 23, no. 2, p. 023114, 2013.

[17] I. Dobson, B. Carreras, V. Lynch, and D. Newman, "An initial model of complex dynamics in electric power system blackouts," in *Proc. 34th Annu. Hawaii Int. Conf. System Sciences, 2001*, 2001, pp. 710–718.

[18] S. Mei, F. He, X. Zhang, S. Wu, and G. Wang, "An improved OPA model and blackout risk assessment," *IEEE Trans. Power Syst.*, vol. 24, no. 2, pp. 814–823, May 2009.

[19] J. Qi and S. Mei, "Blackout model considering slow process and SOC analysis," in *Proc. 2012 IEEE Power and Energy Society General Meeting*, 2012, pp. 1–6.

[20] B. Carreras, D. Newman, I. Dobson, and A. Poole, "Evidence for self-organized criticality in a time series of electric power system blackouts," *IEEE Trans. Circuits Syst. I: Reg. Papers*, vol. 51, no. 9, pp. 1733–1740, 2004.

[21] I. Dobson, B. A. Carreras, V. E. Lynch, and D. E. Newman, "Complex systems analysis of series of blackouts: Cascading failure, critical points, and self-organization," *Chaos: Interdiscipl. J. Nonlin. Sci.*, vol. 17, no. 2, p. 026103, 2007.

[22] B. A. Carreras, V. E. Lynch, I. Dobson, and D. E. Newman, "Critical points and transitions in an electric power transmission model for cascading failure blackouts," *Chaos: Interdiscipl. J. Nonlin. Sci.*, vol. 12, no. 4, pp. 985–994, 2002.
[23] M. Rios, D. Kirschen, D. Jayaweera, D. Nedic, and R. Allan, "Value of security: Modeling time-dependent phenomena and weather conditions," *IEEE Trans. Power Syst.*, vol. 17, no. 3, pp. 543–548, Aug. 2002.
[24] D. Kirschen, D. Jayaweera, D. Nedic, and R. Allan, "A probabilistic indicator of system stress," *IEEE Trans. Power Syst.*, vol. 19, no. 3, pp. 1650–1657, Aug. 2004.
[25] I. Dobson, B. Carreras, and D. Newman, "A probabilistic loading-dependent model of cascading failure and possible implications for blackouts," in *Proc. 36th Annu. Hawaii Int. Conf. System Sciences, 2003*, 2003, vol. 19, no. 01, pp. 15–32.
[26] B. Stott, J. Jardim, and O. Alsac, "Dc power flow revisited," *IEEE Trans. Power Syst.*, vol. 24, no. 3, pp. 1290–1300, Aug. 2009.
[27] R. Zimmerman, C. Murillo-Sanchez, and R. Thomas, "Matpower: Steady-state operations, planning, and analysis tools for power systems research and education," *IEEE Trans. Power Syst.*, vol. 26, no. 1, pp. 12–19, Feb. 2011.
[28] R. Baldick, "Variation of distribution factors with loading," *IEEE Trans. Power Syst.*, vol. 18, no. 4, pp. 1316–1323, Nov. 2003.
[29] M. Eppstein and P. Hines, "A "random chemistry" algorithm for identifying collections of multiple contingencies that initiate cascading failure," *IEEE Trans. Power Syst.*, vol. 27, no. 3, pp. 1698–1705, Aug. 2012.
[30] P. Kundur, *Power System Stability and Control*. Noida, India: Tata McGraw-Hill Education, 1994.
[31] D. N. Kosterev, C. W. Taylor, and W. A. Mittelstadt, "Model validation for the August 10, 1996 WSCC system outage," *IEEE Trans. Power Syst.*, vol. 14, no. 3, pp. 967–979, Aug. 1999.
[32] R. Zarate-Minano, T. Van Cutsem, F. Milano, and A. Conejo, "Securing transient stability using time-domain simulations within an optimal power flow," *IEEE Trans. Power Syst.*, vol. 25, no. 1, pp. 243–253, Feb. 2010.
[33] Y. Xu, Z.-Y. Dong, K. Meng, J. H. Zhao, and K. P. Wong, "A hybrid method for transient stability-constrained optimal power flow computation," *IEEE Trans. Power Syst.*, vol. 27, no. 4, pp. 1769–1777, Nov. 2012.
[34] H. Ren, I. Dobson, and B. Carreras, "Long-term effect of the n-1 criterion on cascading line outages in an evolving power transmission grid," *IEEE Trans. Power Syst.*, vol. 23, no. 3, pp. 1217–1225, Aug. 2008.
[35] Final Report on the August 14, 2003 Blackout in the United States and Canada: Causes and Recommendations, Apr. 2004, Tech. Rep.
[36] R. Pfitzner, K. Turitsyn, and M. Chertkov, "Statistical classification of cascading failures in power grids," in *Proc. 2011 IEEE Power and Energy Society General Meeting*, 2011, pp. 1–8.
[37] R. Pfitzner, K. Turitsyn, and M. Chertkov, "Controlled Tripping of Overheated Lines Mitigates Power Outages," *ArXiv e-prints*, Apr. 2011.
[38] D. Bienstock, "Optimal adaptive control of cascading power grid failures," *ArXiv e-prints*, Dec. 2010.
[39] Y. Fu, M. Shahidehpour, and Z. Li, "Ac contingency dispatch based on security-constrained unit commitment," *IEEE Trans. Power Syst.*, vol. 21, no. 2, pp. 897–908, May 2006.
[40] J. Yan, Y. Zhu, H. He, and Y. Sun, "Revealing temporal features of attacks against smart grid," in *Proc. 2013 IEEE PES Innovative Smart Grid Technologies (ISGT)*, pp. 1–6, to be published.
[41] Y. Zhu, J. Yan, Y. Sun, and H. He, "Risk-aware vulnerability analysis of electric grids from attacker's perspective," in *Proc. 2013 IEEE PES Innovative Smart Grid Technologies (ISGT)*, pp. 1–6, to be published.
[42] J. Arroyo and A. Conejo, "Modeling of start-up and shut-down power trajectories of thermal units," *IEEE Trans. Power Syst.*, vol. 19, no. 3, pp. 1562–1568, Aug. 2004.
[43] Invitation for Low Cost Renewable Energy Projects on Oahu Through Request for Waiver From Competitive Bidding, Feb. 2013 [Online]. Available: http://www.hawaiianelectric.com/vcmcontent/GenerationBid/HECO/CompetitiveBid/ATTACHMENT_1.pdf
[44] F. Milano, "An open source power system analysis toolbox," *IEEE Trans. Power Syst.*, vol. 20, no. 3, pp. 1199–1206, Aug. 2005.
[45] M. Pai, *Energy Function Analysis for Power System Stability*. New York, NY, USA: Springer, 1989.
[46] A. Karami and S. Esmaili, "Transient stability assessment of power systems described with detailed models using neural networks," *Int. J. Elect. Power Energy Syst.*, vol. 45, no. 1, pp. 279–292, 2013.
[47] B. Pal and B. Chaudhuri, *Robust Control in Power Systems*. New York, NY, USA: Springer, 2005.
[48] P. Kundur, J. Paserba, V. Ajjarapu, G. Andersson, A. Bose, C. Canizares, N. Hatziargyriou, D. Hill, A. Stankovic, C. Taylor, T. Van Cutsem, and V. Vittal, "Definition and classification of power system stability IEEE/CIGRE joint task force on stability terms and definitions," *IEEE Trans. Power Syst.*, vol. 19, no. 3, pp. 1387–1401, Aug. 2004.
[49] J. Yan, Y. Yang, W. Wang, H. He, and Y. Sun, "An integrated visualization approach for smart grid attacks," in *Proc. 2012 3rd Int. Conf. Intelligent Control and Information Processing (ICICIP)*, Jul. 2012, pp. 277–283.
[50] H. Ren, X. Fan, D. Watts, and X. Lv, "Early warning mechanism for power system large cascading failures," in *Proc. 2012 IEEE Int. Conf. Power System Technology (POWERCON)*, 2012, pp. 1–6.

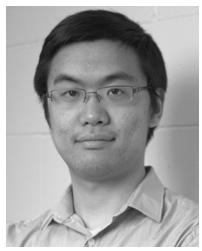

Jun Yan (S'13) received the B.S. degree in information and communication engineering from Zhejiang University, Hangzhou, China, in 2011 and the M.S. degree in electrical engineering from the University of Rhode Island, Kingston, RI, USA, in 2013. He is currently pursuing the Ph.D. degree in the Department of Electrical, Computer and Biomedical Engineering at the University of Rhode Island.

His research interest includes smart grid security analysis, cyber-physical systems and cyber-security, data analysis, computer vision, behavior analysis, computational intelligence, and machine learning. He works with the Laboratory of Computational Intelligence and Self-Adaptive Systems (CISA).

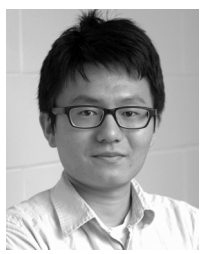

Yufei Tang (S'13) received the B.Eng. and M.Eng. degrees in electrical engineering from Hohai University, Nanjing, China, in 2008 and 2011, respectively. He is currently pursuing the Ph.D. degree at the Department of Electrical, Computer, and Biomedical Engineering, University of Rhode Island, Kingston, RI, USA.

His research interests include power system modeling, power system stability control, wind energy generation and integration, smart grids, power system cyber security, and the application of computational intelligence in power systems.

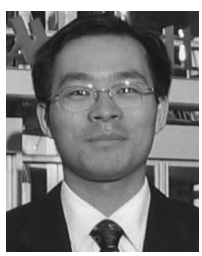

Haibo He (SM'11) received the B.S. and M.S. degrees in electrical engineering from Huazhong University of Science and Technology (HUST), Wuhan, China, in 1999 and 2002, respectively, and the Ph.D. degree in electrical engineering from Ohio University, Athens, OH, USA, in 2006.

From 2006 to 2009, he was an Assistant Professor in the Department of Electrical and Computer Engineering, Stevens Institute of Technology, Hoboken, NJ, USA. He is currently the Robert Haas Endowed Professor in Electrical Engineering at the University of Rhode Island, Kingston, RI, USA. His research interests include smart grid, cyber security, cyber physical systems, adaptive dynamic programming (ADP), machine learning, and computational intelligence and applications. He has published one research book (Wiley), edited 1 research book (Wiley-IEEE) and 6 conference proceedings (Springer), and authored and co-authored over 140 peer-reviewed journal and conference papers. His researches have been covered by national and international media such as IEEE Smart Grid Newsletter, The Wall Street Journal, and Providence Business News.

Prof. He is currently an Associate Editor of the IEEE TRANSACTIONS ON NEURAL NETWORKS AND LEARNING SYSTEMS and the IEEE TRANSACTIONS ON SMART GRID. He was the recipient of the IEEE Computational Intelligence Society (CIS) Outstanding Early Career Award (2014), K. C. Wong Research Award, Chinese Academy of Sciences (2012), National Science Foundation (NSF) CAREER Award (2011), Providence Business News (PBN) "Rising Star Innovator" Award (2011), and Best Master Thesis Award of Hubei Province, China (2002).

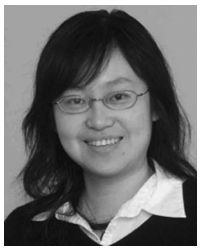

Yan (Lindsay) Sun (M'04) received the B.S. degree with the highest honor from Peking University, Beijing, China, in 1998, and the Ph.D. degree in electrical and computer engineering from the University of Maryland, College Park, MD, USA, in 2004.

She joined the University of Rhode Island, Kingston, RI, USA, in 2004, where she is currently an Associate Professor in the Department of Electrical, Computer and Biomedical Engineering. Her research interests include cyber security, trustworthy cyber-physical systems, and network security. She co-authored the book *Network-Aware Security for Group Communications* (New York, NY, USA: Springer, 2007).

Dr. Sun is an elected member of the Information Forensics and Security Technical Committee (IFS-TC), in the IEEE Signal Processing Society. She has been an associate editor of the IEEE SIGNAL PROCESSING LETTERS since 2013, and an associate editor of Inside Signal Processing eNewsletter since 2010. She was the recipient of NSF CAREER Award (2007), and also recipient of the best paper award at the IEEE International Conference on Social Computing (SocialCom'10).